Experimental Investigation of the Flow Properties of Rarefied Hypersonic Plasma Jets.

- Fabry-Pérot interferometry and Laser Induced Fluorescence -

S. Mazouffre[†], *E. Pawelec*[‡], *V. Caubet-Hilloutou*[†], *M. Dudeck*[†].

[†] Laboratoire d'Aérothermique, CNRS, 1C av. de la Recherche Scientifique, 45071 Orléans, France
[‡] University of Opole, Oleska 48, Opole, Poland

mazouffre@cnrs-orleans.fr/Fax: +33 2 38 25 77 77

Abstract

The flow properties of a low-pressure weakly ionized hypersonic argon plasma jet are examined using Fabry-Pérot interferometry and Laser Induced Fluorescence spectroscopy. The line profile of two Ar lines at 763 nm and 738 nm respectively, are analysed by means of a plane Fabry-Pérot interferometer. The velocity is obtained from the Doppler shift of the line and the temperature is deduced from the Doppler broadening of the peak. The LIF experiment is based on the use of a tunable single mode laser diode. Laser excitation of the resonant Ar[$1s_4$] level at 810 nm allows to locally measure the velocity distribution function of Ar atoms both in radial and axial direction. The plasma flow is found to be already supersonic inside the arcjet nozzle, with a Mach number of 3.5 at the exhaust. The flow velocity reaches 5 km s^{-1} in the supersonic domain. The gas temperature is 1700 K at the nozzle outlet, T = 600 K ahead of the shock wave and it rises up to 3500 K in the shock region.

1 Introduction

One convenient way of improving our understanding of the physics of the interaction between an hypersonic vehicle and a surrounding medium is to conduct ground-based experiments in order to collect a large set of data that are critically analyzed and compared with theoretical expectations and numerical outcomes. It is nowadays well-established that low-pressure weakly ionized hypersonic plasma jets can serve as a simulation tool for some of the specific conditions encountered during high speed flights in planetary atmospheres. At present, fields of interest are hypersonic flight in the upper layers of the Earth's atmosphere [1] and entry of a space probe in the Mars atmosphere [2]. Knowledge about the properties of the plasma that is created in front of the vehicle for a given atmosphere composition and a given trajectory is necessary for instance for optimization of the vehicle's thermal shield and for determination of the plasma frequency which drives attenuation in radio transmissions.

In this contribution, we mainly examine the flow properties of a hypersonic plasma jets employing various diagnostic tools. All mentioned studies are being performed with the SR5 plasma wind tunnel equipped with a dc arcjet, a ground-based facility located at the Laboratoire d'Aérothermique in Orléans [1]. This kind of plasma wind-tunnel offers two advantages: The easiness of probing the jet owing to its large size, and stationary flow conditions. Studies performed in Orléans are complementary to studies carried out at the university of Marseille with the TCM2 shock tube and at the ONERA institute in Toulouse with the F4 pulsed wind-tunnel as only a part of the whole hypersonic flight domains can be simulated with the SR5 facility.

In order to characterize the SR5 facility in terms of flow velocity, streamline temperature and Mach number, numerous measurements have been performed when running the arcjet on argon. Note that a small fraction of nitrogen is added to the argon gas flow to limit the production of Ar ions. Such an experiment can be considered as a test case, in the sense that the absence of a complex chemistry makes easier the understanding of the observed phenomena. The electron density along the jet axis is measured in the plasma plume by means of cylindrical electrostatic probe. Analysis of two Ar line profiles with a Fabry-Pérot interferometer allows to ob-

tain the plasma temperature and flow velocity in the direction of observation. Finally, a Laser Induced Fluorescence (LIF) spectroscopy technique based on a tunable laser diode is used to locally probe the velocity distribution function of a resonant Ar state from which the velocity and the temperature can be inferred.

2 Arcjet and plasma plume

The plasma source used in the SR5 ground-test facility is a water-cooled vortex stabilized dc-arc torch [1, 3]. The torch is equipped with a tungsten cathode and with a convergent (30°)-divergent (25°) copper nozzle that acts as a grounded anode. The length of the divergent part is 5 cm and the exit diameter of the nozzle is 4.8 cm. The arc extends from the tip of the cathode through a 4 mm diameter molybden throat and attaches diffusely to the nozzle. The arcjet can be operated in a wide range of currents (10 to 300 A) and flows (5 to 50 slm). The plasma torch can be run for several hours, the lifetime being determined by the cathode erosion. Gases are fed through mass flow controllers directly into the cathode area. The torch is mounted on an arm that can be moved in vertical and horizontal direction. A thermal plasma is created in an Ar-N_2 gas mixture. Subsequently the plasma expands from the arcjet into a low pressure stainless steel vessel. The vacuum chamber is 4.3 m long and has a diameter of 1.1 m. The pumping capacity can be varied by means of a valve, and in this way the residual pressure can be changed almost independently from the gas flow. Standard operating conditions for this experiment are: a 100 A direct current, a cathode-anode voltage of 45 V, an Ar gas flow of 20 slm (0.6 $\mathrm{g\,s^{-1}}$) and a N_2 gas flow of 5 slm (0.1 $\mathrm{g\,s^{-1}}$). The pressure in the cathode area is 76 kPa and the background pressure is 2.5 Pa. The cathode to anode gap is 1 mm. The efficiency is around 60% and the specific enthalpy is 3.8 $\mathrm{kJ\,g^{-1}}$, i.e. 1.5 eV per particle assuming that the furnished energy is entirely converted into temperature.

A detailed description of the physics of free plasma jets is available elsewhere [4]. Here only a short overview of the expansion picture is presented. Because the plasma expands through a nozzle from a high pressure region into a low pressure region, a well-defined free jet shock wave structure is produced, as depicted in Fig. 1. The plasma first flows supersonically (M=1 at the nozzle throat and the flow is already supersonic in the divergent section). In this flow domain, the temperature drops in accordance with the Poisson adiabatic law and the drift velocity increases due to energy conservation. In the mean time, the particle density along a streamline decreases because of the increase in the jet diameter, the so-called rarefaction effect. At some distance from the source, depending among others upon the background pressure, a normal stationary shock wave, or compression wave, is formed to allow the flow to adapt to the ambient gas conditions. Throughout the shock region, of which dimensions are in the order of the local neutral-neutral collision mean free path, the flow undergoes a transition from a supersonic regime to a subsonic regime. The flow is strongly decelerated across the shock wave. As a consequence, the temperature increases because of energy conservation, and the density increases. Behind the shock wave, the plasma flows subsonically and at constant static pressure. The supersonic domain is surrounded by a so-called stationary barrel shock wave. Deviation from the classical free jet flow picture may appear in the case of transient species like radicals and charged particles [4].

The electron density development along the plasma plume centerline is shown in Fig 2. The density has been measured using a cylindrical Langmuir probe (100 μm diameter) placed parallel to the flow direction [5]. The electron density has been determined from the probe voltage-current characteristics assuming that $T_e \approx T_{Ar}$. The ionization degree at the nozzle exit is below 10^{-3} ($n_{Ar} \approx 10^{22}\,\mathrm{m^{-3}}$ at the exhaust, after [3]). The relatively low ion content in the jet is due to the addition of a small fraction of N_2 to the Ar gas flow (see section 5). The electron density decreases in the course of the plasma expansion. The jump in density at $z = 15$ cm may be a consequence of the formation of a bow shock wave around the probe. The electron density measured in the first centimeters must be considered with care for three main reasons. First, the Langmuir probe is an intrusive method, i.e. it disturbs the supersonic flow [5], especially in regions where the pressure is still high. Second, the probe experiences a large heat flux, which can lead to a change in the probe electric properties. Third, the Ar ion drift velocity is much higher than the Ar ion thermal speed, in contradiction with the classi-

cal Langmuir probe theory [6]

3 Fabry-Pérot interferometry

3.1 Fabry-Pérot bench

A Fabry-Pérot (FP) interferometer must be regarded as a very narrow bandwidth optical filter [7, 8]. It is often used to examine the detailed structure of spectral lines. A schematic view of the complete Fabry-Pérot system is depicted in Fig 3. After being collected with a lens, light emanating from the plasma jet is transported towards the optical bench by means of a multimode optical fiber with a 365 μm core diameter. A similar fiber is also used to carry part of the light emitted by a 100 Hz low pressure argon lamp. The two optical fibers arc combined by means of a three ports 50/50 fiber coupler. The light leaving the fiber is collected with a 400 mm focal distance lens in such a way that a collimated beam of light is created. The parallel beam passes a plane Fabry-Pérot cavity limited by two 2.5 cm diameter apertures. Behind the cavity, the transmitted light is focused onto a 0.7 mm pinhole in order to solely select the central interference ring. The pinhole is imaged onto the entrance slit of a 40 cm monochomator that acts as a rough wavelength selector to separate the line to be studied from the remainder of the spectrum ($\Delta\lambda \approx 0.8$ nm). A photomultiplier tube (Hamamatsu R955) is used as a light detector. The delivered signal is register with an oscilloscope connected to a computer. The Fabry-Pérot (RC110 from Burleigh) is a piezo-scanned type: The length as well as the alignment of the cavity is controlled by applying a high voltage onto piezoelectric mirror mounts. An accurate frequency scan is realized by smoothly varying the mirror position with a high voltage ramp. All measurements presented in this paper have been obtained with a cavity scanning frequency of 10 Hz. Each spectrum results from the average over 500 cycles.

The distance between the two dielectric mirrors of the Fabry-Pérot cavity is 15.1 mm, meaning that the Free Spectral Range of the cavity is equal to 9.924 GHz. In the spectral range of interest, the mirror reflectivity is around 99%. The mirrors are flattened to $\lambda/200$. Therefore, the net finesse of the FP cavity is around 180. The instrumental finesse that characterizes the resolving power of the complete FP bench by accounting for pinholes and lenses induced losses, is found to be around 65 [7]. In other words, the FP setup allows to achieve a spectral resolution of about 0.15 GHz (0.4 pm). Light emitted by a low-pressure argon lamp is used as a calibration tool. Analyzing the profile of an Ar line of which the Doppler width is accurately known allows to check the instrumental finesse, i.e. the apparatus profile of the FP setup [7]. Moreover, Ar atoms being on the average at rest in the lamp, the latter is also used as a reference for null velocity, i.e. for the zero Doppler shift position (see Fig. 4).

The experimental arrangement used to collect the light emitted by the plasma jet is depicted in Fig. 5. A lens with a 100 mm focal distance images the jet onto the entrance of a multimode optical fiber connected to the Fabry-Pérot bench. The magnification is 0.125 that corresponds to a spatial resolution of 3 mm in radial direction. The line of sight is oriented either at 90° or at 60° with respect to the jet symmetry axis. With the first configuration, one can measure both the perpendicular temperature (associated with the velocity distribution perpendicular to a stream line) and the radial velocity component. Note that, in case of an axial symmetry flow, the existence of a perpendicular velocity component leads to an artificial broadening of the observed emission peak. Using the second configuration, one obtains the axial velocity component after correction with the cosine of the angle. As it will be discussed in the last section, such a configuration allows to probe the plasma flow inside the nozzle of the arcjet. Fabry-Pérot spectroscopy does not allow to carry out measurements with a good spatial resolution. The field depth of the observation branch is 25 cm, i.e. the field depth is larger than the plasma jet diameter. As a consequence, the obtained line profile corresponds to the one integrated along the line of sight.

3.2 FP lineshape analysis

Two Ar line profiles are analyzed with the Fabry-Pérot setup. The Ar I line at 763.51 nm corresponds to the $2p_6 \rightarrow 1s_5$ transition. The Ar I line at 738.40 nm corresponds to the $2p_3 \rightarrow 1s_4$ transition. Note that the $1s_5$ state is metastable whereas the $1s_4$ state is resonant. These two Ar lines offer several advantages: They are well isolated, they both correspond to a relatively strong transition, and the PMT quantum efficiency is relatively high below

800 nm. As already mentioned, the temperature can be deduced from the Doppler broadening of the line taking into account the apparatus width [7]. The Doppler shift of the observed line allows to determine the mean velocity in the direction of observation.

As can be seen in Fig. 4, when the seeded N_2 fraction is small, radiation is strongly reabsorbed around the spectral line center due to the production of a large number of excited Ar atoms in the plasma plume. This fact is especially true for the 763 nm Ar line that is linked to the longlived Ar[$1s_5$] state.

4 Laser Induced Fluorescence

4.1 cw-LIF setup

A schematic of the Laser Induced Fluorescence setup is depicted in Fig. 6. A single mode tunable external cavity diode laser (SACHER TEC 500 in Littman configuration) delivers about 30 mW of vertically polarized near-infrared radiation (800 nm to 830 nm) with a bandwidth of 0.5 MHz. A Faraday isolator prevents any reflected beam of light to enter back into the laser cavity. A small fraction of the beam is passed through a low-pressure argon lamp. The absorption spectrum measured in that way is used to define the unshifted frequency position. A second beam splitter directs a small part of the laser into a 3.3 GHz Fabry-Pérot etalon to monitor mode structure and ensure that no mode hop occurs during operation. The mode-hop free tuning range of the laser is typically 30 GHz with voltage-current coupling. The recorded transmission of the Fabry-Perot etalon is also used to linearize the frequency axis. The laser beam is coupled into a single mode optical fiber with a 5 μm core diameter using a 4 mm focal distance lens. Such a device allows to obtain a 30% coupling efficiency without shaping the beam. Two excitation configurations are possible. In one configuration using a metal (gold) mirror located inside the vacuum chamber, the laser beam propagates opposite to the plasma flow direction at a 30° angle with respect to the jet axis. In another configuration the beam is directed perpendicular to the flow direction. In both cases a 4 mm focal distance lens is used to focus the beam leaving the optical fiber onto the axis. The beam waist is estimated to be around 2 mm.

The laser light is chopped at a frequency of about 200 Hz and the laser induced fluorescence signal is detected on a horizontal axis normal to both excitation directions. The signal is collected with two lenses (f_1 = 100 cm and f_2 = 20 cm) and imaged onto a Hamamatsu R928 photomultiplier tube (PMT). A narrow bandwidth interference filter centered at 810 nm is placed in front of the detector to filter out extraneous plasma light. A 0.5 mm aperture mounted directly in front of the detector at the focal plane of the imaging lens system determines the spatial resolution. The magnification is equal to 4, hence the resolution in horizontal direction is around 2 mm. Phase-sensitive detection is used to discriminate the fluorescence light from the intrinsic plasma emission which is about 1000 times greater. The signal delivered by the PMT is analyzed with a lock-in amplifier which is synchronyzed to the chopper frequency. The integration time of the lock-in amplifier is 500 ms. All signals are recorded simultaneously with a 16 bit 333 kHz analog-to-digital converter (National Instruments PCI-6052E). The scanning of the laser frequency is controlled by supplying a low voltage to the piezoelectric block connected to the end mirror of the laser diode cavity. Typical scan times are several minutes.

4.2 LIF measurements

All LIF measurements presented in this paper correspond to excitation of the Ar[$1s_4$] resonant level. The laser frequency is scanned over the $1s_4 \rightarrow 2p_7$ transition at 810.37 nm. Four raw waveforms obtained with the LIF diagnostic tool after radial excitation are shown in Fig. 7. As can be seen, the absorption spectrum across the plasma jet is similar to the absorption spectrum in a low pressure Ar lamp in terms of peak shape and position. It implies that the flow is axisymmctric. It also demonstrates that the jet can be used as a stationary reference for determining the zero Doppler shift. As shown in Fig. 7, the laser power varies during a scan over the Ar transition. LIF profiles must therefore be corrected in order to obtain the proper baseline.

The bandwidth of the laser is in the order of 0.5 MHz, much narrower than the width of the measured Ar profiles (few GHz in the plasma plume). Hence, a recorded spectral profile is a direct measurement of the Ar atom velocity distribution function along the laser beam axis. The local mean Ar atom velocity is deduced from the line profile. If the system is in

thermodynamic equilibrium (Gaussian distribution), an Ar atom temperature can be defined (related to the width of the line). The area of the peak provides a direct measure for the local Ar[$1s_4$] density.

5 Interpretation of measured spectra

Under our experimental conditions, light emitted by the plasma jet mostly originates in the radiative deexcitation of Ar atom excited states formed in a three particle recombination process involving Ar ions

$$Ar^+ + e + e \rightarrow Ar^* + e. \quad (1)$$

Therefore, the flow properties of the probed excited Ar* atoms image in first instance the behavior of Ar^+ ions. Note that it is well known that all Ar* atoms produced in this way cascade down to the $4s$ multiplet [9]. However, it has been shown that in case of an argon plasma expansion, the behavior of Ar^+ ions is strongly linked to the behavior of Ar atoms [9]. In other words, monitoring the Ar* atoms properties is an indirect way of determining the properties of Ar atoms, i.e. an indirect way of obtaining the plasma flow properties since ground-state Ar atoms are the major species in the jet. A detailed explanation of the Ar^+-Ar coupling in a plasma jet can be found in reference [9]. Here we briefly summarize the main ideas. The mean free path for momentum exchange between two groups of particles is calculated according to the following relation

$$\lambda = \frac{v}{n\sigma v_{th}}, \quad (2)$$

where v is the species flow velocity, n is the density of the collision partner, σ is the collision cross-section and v_{th} is the thermal speed. At the nozzle exit the Ar atom density is roughly equal to 10^{22} m^{-3} [3]. Thus the Ar^+-Ar collision length λ_{Ar^+-Ar} is below 1 mm and $\lambda_{Ar-Ar} \approx 3$ mm. Ahead of the shock region, one finds $\lambda_{Ar^+-Ar} \approx 5$ cm and $\lambda_{Ar-Ar} \approx 20$ cm. In all cases, the mean free path is less than any gradient scale length. The acceleration of Ar ions that results from the existence of a local electric field generated from gradients in charge density can be neglected [4]. First, the magnitude of the field is extremely low in the jet. Second, the collision frequency is still high enough at the nozzle exit to forbid Ar^+ to be accelerated without enduring any collision. A last effect is also of importance, especially in the case of LIF measurements. Under our experimental conditions, due to the VUV radiation trapping resonant and ground-state argon atoms are very efficiently coupled and can therefore be considered as being fully mixed [9]. This means that the velocity distribution of resonant Ar[$1s_4$] atoms and ground-state Ar atoms are identical.

Addition of a small fraction of molecular nitrogen simply permits to limit both the emission and the reabsorption of infrared light. It has no influence upon the overall plasma flow characteristics. The efficient charge exchange reaction between Ar atoms and N_2^+ ions

$$Ar^+ + N_2 \rightarrow Ar + N_2^+, \quad (3)$$

leads to the disappearance of a large number of Ar^+ ions, which are at the origin of the existence of Ar* atoms as aforementioned. Reaction 3 is followed by the fast dissociative recombination of the formed N_2^+ molecular ion [10].

6 Rarefied plasma jet properties

6.1 Temperature

As already mentioned, the temperature is obtained from the Doppler broadening of the observed Ar spectral lines. In view of the low electron density, see Fig. 2, Stark broadening can be neglected for all considered Ar states [12]. Moreover, collisional broadening is negligible in the pressure range of interest. Therefore, the Doppler effect appears to be the main broadening mechanism.

The development of the perpendicular temperature along the jet centerline has been measured with the FP setup, as can be seen in Fig. 8. The temperature decreases from 3500 K at the nozzle outlet down to 2500 K around $z = 14$ cm as the result of the expansion process. A temperature measured by means of FP interferometry must, however, be considered as an upper limit of the real local temperature, as already explained in section 3. The last part of the temperature profile exhibits a plateau-like structure. This region, where the temperature is constant, corresponds to the zone of silence, which is the region located ahead of the stationary shock wave [4]. Measurements have not been performed further downstream due to a too

weak Ar light intensity. The radial profile of the perpendicular temperature obtained at the nozzle outlet is shown in Fig. 9. The profile is symmetric and the temperature is highest on the jet axis. This measurement reveals the existence of a strong temperature gradient between the core of the jet and its vicinity. In other words, the plasma jet is surrounded by a relatively cold gas.

The Ar atom perpendicular temperature has also been determined by means of LIF spectroscopy. In Fig. 10, the on-axis profile of the temperature indicates that the temperature decreases between $z = 0$ cm and $z = 13$ cm, in agreement with the FP measurements. The LIF technique, however, enable to obtain more accurate values of macroscopic quantities such as the temperature (see section 10). In comparison with results shown in Fig. 8, one can observed in Fig. 10 that the plasma temperature is relatively low behind the nozzle exit and that the temperature drop is quite pronounced. The temperature in the zone of silence is only 600 K. An abrupt temperature rise occurs throughout the shock wave due to conversion of kinetic energy into thermal energy [4]. The remainder of the temperature profile will soon be measured by LIF in order to probe the complete shock region and to examine the subsonic flow domain. A radial profile of the perpendicular Ar atom temperature measured by LIF at $z = 10$ cm is depicted in Fig. 11. The temperature can be considered as homogeneous over the jet diameter with a value of around 1200 K. The large scatter in the measured data may originate in plasma plume fluctuations.

6.2 Flow velocity

The radial profile of the Ar atom radial velocity component has been measured by LIF at $z = 10$ cm, see Fig. 11. The velocity is zero on the jet axis, and it reaches 600 m s^{-1}, which is its maximum value, at $r = \pm 3$ cm. This position defines the start of the barrel shock wave [4]. The shape of the profile confirms the axisymmetry of the plasma jet. The velocity returns back to zero at $r = 8$ cm. This position can be considered as the jet boundary. Thus the expansion angle is found to be 28°, which almost corresponds to the nozzle opening angle. The core of the plasma jet, i.e. the region limited by the barrel shock, expands with an angle of 11°.

So far, the axial velocity has only been measured by means of Fabry-Pérot interferometry. In Fig. 12, the plasma flow velocity is plotted against the position along the jet axis. Surprisingly, the velocity is found to be constant in the investigated zone with a magnitude of 4.5 km s^{-1}. The axial velocity is expected to slightly increase as a direct consequence of the temperature decrease [4, 9]. This unexpected point may find its origin in the fact that FP measurements are integrated along the line of sight and do not represent local value. Also shown in Fig. 12 is the speed of sound calculated from the temperature measured with a 60° line of sight. The local speed of sound reads

$$c_s = \sqrt{\frac{\gamma k_B T}{m}}, \tag{4}$$

where γ is the specific heat ratio, k_B is the Boltzmann constant, T is the temperature and m is the mass of the specie. In case of a 4:1 Ar-N_2 mixture, $\gamma = 1.6$ and $m = 37.6$ amu. The speed of sound drops from 1.5 km s^{-1} downto 1 km s^{-1} owing to cooling of the flow. The axial profile of the Mach number M is presented in Fig. 13. The Mach number is simply the v/c_s ratio. The increase in M originates in the lowering of the plasma temperature. Contrary to expectation, it is not a signature for an acceleration of the flow. The flow is already supersonic inside the arcjet nozzle. M is equal to 3.5 at the nozzle exit and M = 4 at $z = 4$ cm.

The radial development of the Ar atom axial velocity component has been measured inside the arcjet nozzle, as can be seen in Fig. 14. The velocity is maximum on-axis and the profile is symmetric. The velocity approaches zero close to the nozzle wall.

6.3 Influence of the supplied power

The evolution of both the Ar atom axial velocity and temperature with the applied electric power is shown in Fig. 15. Measurements have been carried out inside the nozzle with the Fabry-Pérot bench. The velocity as well as the temperature increase with the power whereas the Mach number stays approximately constant with a magnitude of about 3.5. The Ar atom temperature varies linearly with the supplied electric power (thermal and electrical conductivity for argon plasma). As shown, by changing the power, one can change the range of achievable velocity. This is an interesting feature for ground-based simulation of entries in a planetary atmosphere. Indeed, it allows to simulate

a large part of the entry trajectory. From our set of measurements, it follows that in the case of the SR5 facility, the velocity can reasonably be varied from 3 $\mathrm{km\,s^{-1}}$ to 8 $\mathrm{km\,s^{-1}}$ when operating the arcjet on argon. When using molecular gases such as N_2 or CO_2 the velocity is expected to be less as part of the supplied energy is used for dissociation and stored in vibrational excitation. The lifetime of the arcjet is of course shorten when operating at high electric power.

7 Conclusion

The flow properties of a low-pressure weakly ionized argon plasma jet have been determined using Fabry-Pérot interferometry and Laser Induced Fluorescence spectroscopy. The plasma flow is already supersonic inside the arcjet nozzle. The flow velocity reaches 5 $\mathrm{km\,s^{-1}}$ behind the nozzle outlet. The Mach number increases in the course of the expansion as the result of the cooling of the flow. The gas temperature is 1700 K at the nozzle outlet and it drops downto 600 K ahead of the normal shock wave of which the existence is revealed by a sudden temperature rise.

In the very near future, to determine the flow velocity and M behind the nozzle exhaust by means of LIF. Moreover, LIF on metastable $\mathrm{Ar}[1s_5]$ state at 811 nm to be able to probe regions beyond the zone of silence. especially of importance is the measurement of the dimension of the shock, the temperature jump i.e. the amount of energy provided in the shock. We also plan to try to determine the flow velocity using a time of flight method with Langmuir probe and to compare all different techniques.

Acknowledgements

The authors greatly appreciate the technical assistance of O. Antonin. The authors would like to acknowledge fruitful discussions with Dr. V. Lago about the Langmuir probe theory. This work was carried out with the support of the Région Centre.

References

[1] S. Mazouffre, E. Pawelec, V. Lago, M. Lino da Silva, M. Dudeck, *Plasma formation during high speed flights in the upper layers of the Earth's atmosphere*, AIAA paper **02-5272** (2002).

[2] M. Lino da Silva, V. Lago, R. Reis, M. Dudeck, *Modelling and experimental analysis of CO_2/N_2 plasma flows with and without the presence of an obstacle*, AIAA paper **03-3856** (2003).

[3] A. Kamińska, M. Dudeck, *Modelling of non-equilibrium arcjet plasma flow*, J. Tech. Phys. **40**, 33 (1999).

[4] D.C. Schram, S. Mazouffre, R. Engeln, M.C.M. van de Sanden, *The physics of plasma expansions*, in Atomic and Molecular Beams, edited by R. Campargue, Springer, New York, 209 (2001).

[5] R.F.G. Meulenbroeks, M.F.M. Steenbakkers, Z. Qing, M.C.M. van de Sanden, D.C. Schram, *Four ways to determine electron density in low-temperature plasmas*, Phys. Rev. E **49**, 2272 (1994).

[6] W.A. Clayden, *Langmuir probe measurements in the R.A.R.D.E. plasma jet*, in Advances in Applied Mechanics, Rarefied Gas Dynamics, Academic Press, London, vol. 2, p. 435 (1963).

[7] S. Mazouffre, D. Pagon, P. Lasgorseix, M. Touzeau, *Temperature of xenon atoms in a Stationary Plasma Thruster*, Proceedings of the 28^{th} International Electric Propulsion Conference, Toulouse, France (2003).

[8] V.M. Lelevkin, D.K. Otorbaev, D.C. Schram, *Physics of Non-Equilibrium Plasmas*, North-Holland, Amsterdam (1992).

[9] R. Engeln, S. Mazouffre, P. Vankan, D.C. Schram, N. Sadeghi, *Flow dynamics and invasion by background gas of supersonically expanding thermal plasma*, Plasma Sources Sci. Technol. **10**, 595 (2001).

[10] G.J.H. Brussaard, M.C.M. van de Sanden, D.C. Schram, *Ion densities in a high-intensity, low flow nitrogen-argon plasma*, Phys. Plasmas **4**, 3077 (1997).

[11] J.G. Liebeskind, R.K. Hanson, M.A. Cappelli, *Laser-induced fluorescence diagnostic for temperature and velocity measurements in a hydrogen arcjet plume*, Appl. Opt. **30**, 6117 (1993).

[12] D. Schinköth, M. Kock, E. Schulz-Gulde, *Experimental stark broadening parameters for near-infrared Ar I and Kr I lines*, J. Quant. Spectrosc. Radiat. Transfer **64**, 635 (2000).

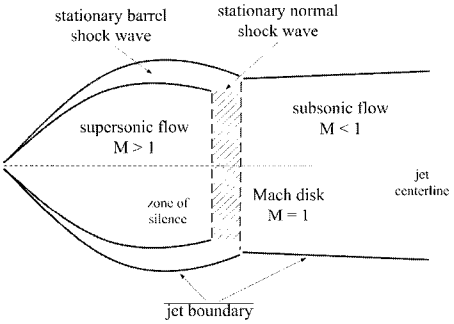

Fig. 1: Sketch of the free plasma jet structure. The plasma first expands supersonically. At some distance from the source a normal shock wave is formed. Behind the shock front the plasma flows subsonically and at constant static pressure. The supersonic flow domain is limited by a barrel shock wave. M refers to the Mach number.

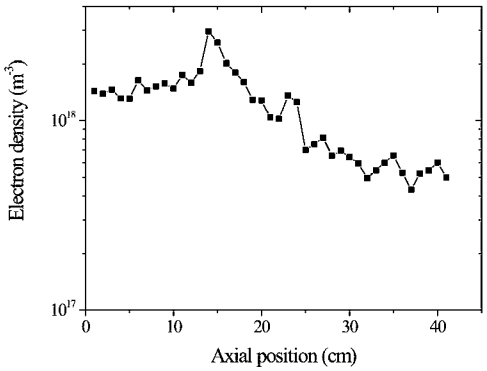

Fig. 2: Axial profile of the electron density measured with a cylindrical Langmuir probe positioned parallel to the flow direction. The electron density decreases in the course of the plasma expansion. The jump in density at $z = 15$ cm may be a consequence of the formation of a bow shock wave around the probe. The ionization degree at the nozzle exit is below 10^{-3} [3]

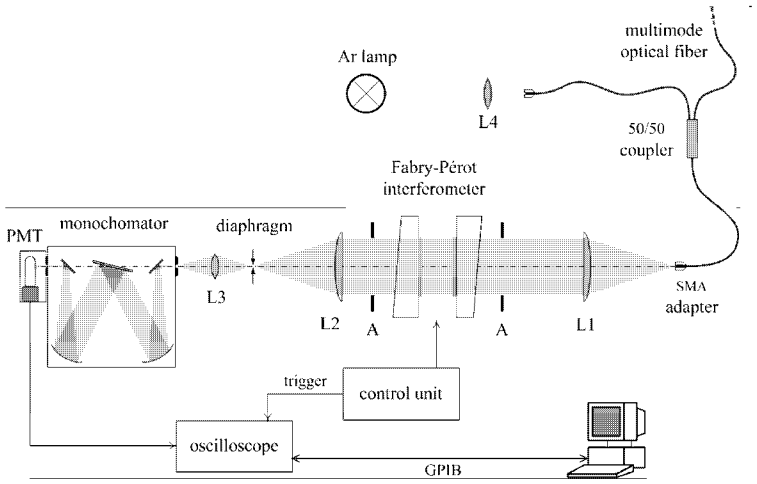

Fig. 3: Schematic view of the emission spectroscopy setup using a plane Fabry-Pérot interferometer. Light issuing from the plasma jet is transported towards the optical bench by means of a multimode optical fiber. The plasma light is mixed with the light of a low pressure argon lamp ($f_4 = 100$ mm) with a 3 ports fiber coupler. The interferometer is placed in the equidistant beam part created between lenses L_1 and L_2 ($f_1 = f_2 = 400$ mm). The Fabry-Pérot active area is defined by two apertures (A). A small diaphragm selects the central ring ($f_3 = 40$ mm). A monochromator selects the spectral line of interest. The PMT signal is recorded by an oscilloscope. A control units enable varying the mirror spacing. The FSR of the interferometer is equal to 9.924 GHz. The calculated net finesse of the setup is approximately 65.

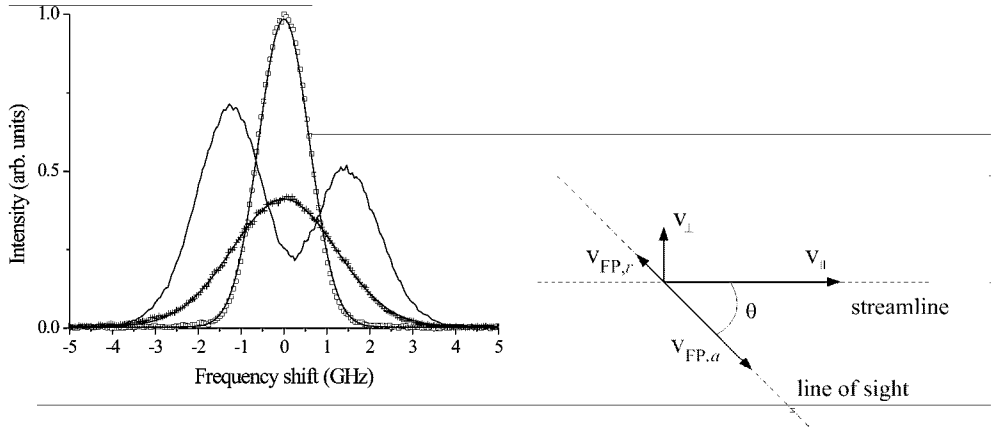

Fig. 4: Profiles of the Ar 763 nm line measured with the FP bench: low pressure argon lamp (square) and arcjet nozzle outlet. In standard conditions, the Ar line profile is Gaussian (cross). When the seeded N_2 fraction is small (solid line) the 763 nm radiation is strongly reabsorbed around the spectral line center.

Fig. 5: Observation configuration for FP interferometry. The line of sight is directed either at 90° or at 60° with respect to the jet centerline. The v_{FP} symbol corresponds to the projection of the velocity onto the line of sight. Collecting the plasma light with such a configuration allows to measure both axial and radial velocity and temperature components.

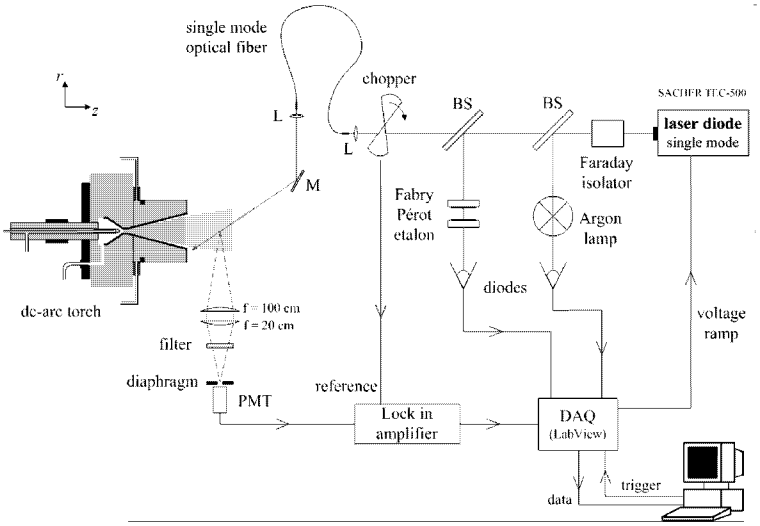

Fig. 6: Schematic view of the experimental cw-LIF setup using a single mode tunable laser diode and phase sensitive detection. The Faraday isolator prevents any back reflexion of the light into the laser cavity. The Ar lamp is used as a velocity reference. A 3.3 GHz Fabry-Pérot etalon is employed to monitor mode hops. The laser light is transported towards the vacuum chamber via a single mode optical fiber. The laser beam can be directed either perpendicular or obliquely (at an angle of 30°) with respect to the flow direction. The map of the plasma plume properties is realized by moving the arcjet.

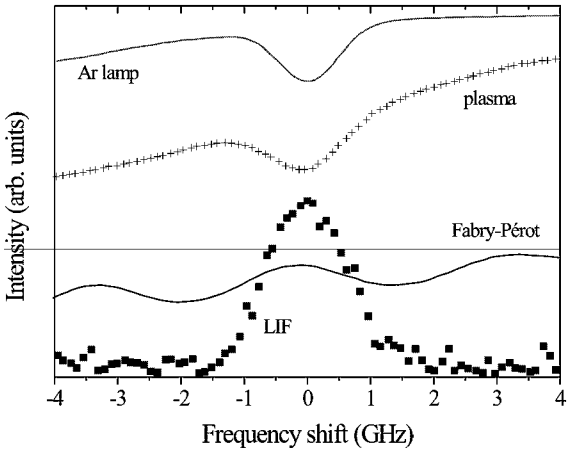

Fig. 7: Raw waveforms obtained with the LIF diagnostic tool: absorption spectrum in a low pressure Ar lamp, absorption spectrum along the plasma jet diameter, transmission of the Fabry-Pérot etalon and fluorescence resulting from excitation of the Ar[$1s_4$] state in the plasma plume. The power of the laser beam can vary up to 20% during a scan over the transition that necessitates to correct the LIF profile.

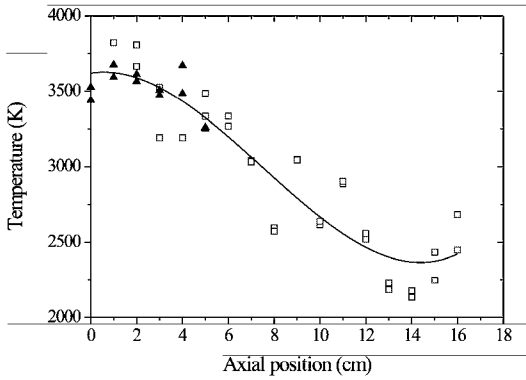

Fig. 8: Perpendicular temperature as a function of axial position measured with the FP setup. Two Ar lines have been analyzed, respectively at 738 nm and 763 nm. The solid line is drawn to guide the eye.

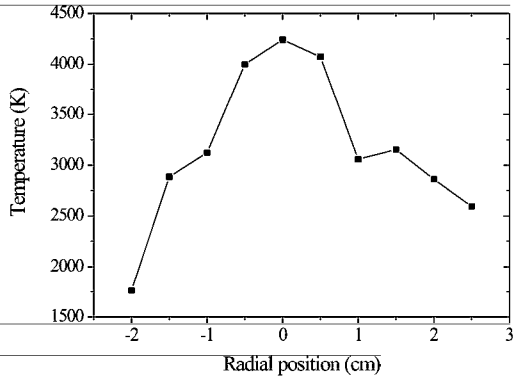

Fig. 9: Perpendicular temperature as a function of radial position measured at the nozzle exhaust with the Fabry-Pérot interferometer.

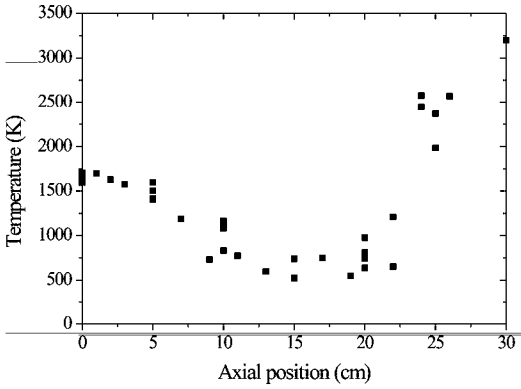

Fig. 10: Development of the perpendicular temperature along the jet axis measured by LIF. An abrupt temperature rise is observed in the shock wave region.

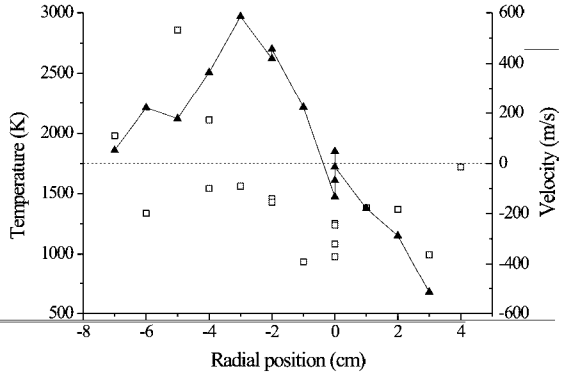

Fig. 11: Perpendicular temperature (square) and radial velocity component (triangle) as a function of the radial position measured by LIF at $z = 10$ cm.

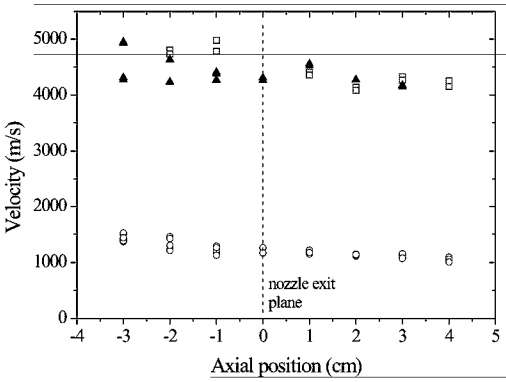

Fig. 12: On-axis profile of the axial velocity component measured by interferometry with the 738 nm (triangle) and 763 nm (square) Ar lines. Also shown is the speed of sound calculated from the measured temperature (circle).

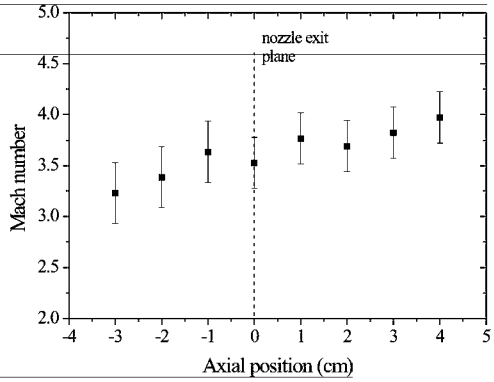

Fig. 13: Mach number as a function of the position along the jet axis. As expected, the flow is already supersonic inside the nozzle. The increase in the magnitude of the Mach number is seemingly due to cooling of the plasma flow.

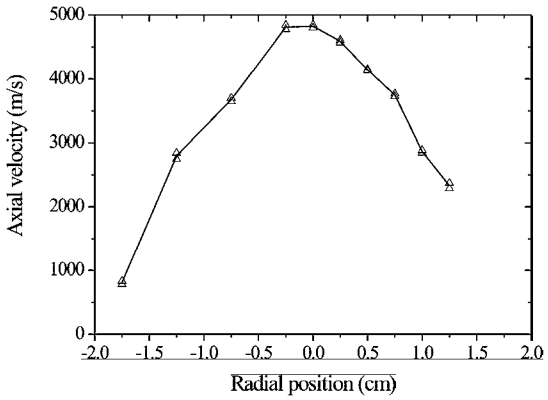

Fig. 14: Radial profile of the axial velocity component measured by interferometry inside the nozzle (z = -2 cm). As expected, the velocity is highest on axis and it is zero near the wall of the arcjet nozzle.

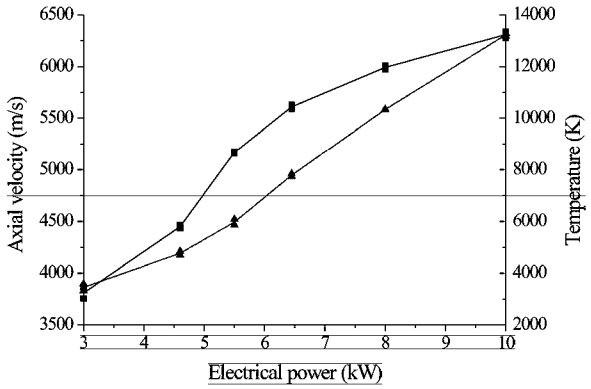

Fig. 15: Temperature (triangle) and axial velocity (square) as a function of the applied electrical power. Measurements realized inside the nozzle (z = -2 cm) by monitoring the 738 nm Ar line profile with the FP interferometer. The temperature varies linearly with the power. The Mach number stays approximately constant (M$\approx$ 3) whatever the power.